

PLANETARY SCIENCE

Aluminum-26 chronology of dust coagulation and early solar system evolution

M.-C. Liu^{1*}, J. Han^{2,3}, A. J. Brearley⁴, A. T. Hertwig¹

Dust condensation and coagulation in the early solar system are the first steps toward forming the terrestrial planets, but the time scales of these processes remain poorly constrained. Through isotopic analysis of small Ca-Al-rich inclusions (CAIs) (30 to 100 μm in size) found in one of the most pristine chondrites, Allan Hills A77307 (CO3.0), for the short-lived ^{26}Al - ^{26}Mg [$t_{1/2} = 0.72$ million years (Ma)] system, we have identified two main populations of samples characterized by well-defined $^{26}\text{Al}/^{27}\text{Al} = 5.40 (\pm 0.13) \times 10^{-5}$ and $4.89 (\pm 0.10) \times 10^{-5}$. The result of the first population suggests a 50,000-year time scale between the condensation of micrometer-sized dust and formation of inclusions tens of micrometers in size. The 100,000-year time gap calculated from the above two $^{26}\text{Al}/^{27}\text{Al}$ ratios could also represent the duration for the Sun being a class I source.

INTRODUCTION

The formation time scale of first solids in the Sun's protoplanetary disk has been of major interest because it is the first step toward the formation of terrestrial planets. Some of our knowledge about planet formation in the solar system is drawn from theories (1) and astronomical observations of protoplanetary disks around young stellar objects (YSOs) (2). However, the spatial resolution of observations of YSOs is insufficient to reveal details inside the disks. In the past few years, our understanding of planet formation in young stellar systems has been revolutionized by the high-spatial resolution observations of HL Tau, a class I/II object, by ALMA (Atacama Large Millimeter/submillimeter Array) (3). The disk around this <1-million year (Ma)-old young star was found to be characterized by a structure composed of several axisymmetric bright and dark rings, indicating ongoing formation of planets or large planetary precursors at this stage of stellar evolution (3, 4), which is a few million years earlier than would be expected from theories (1). One implication of these new findings, which is consistent with that inferred from the tungsten isotopic compositions of iron meteorites (5), is that our solar system could have also started forming rocky planets (or their precursors) as early as hundreds of thousands of years after its formation. It should, however, be noted that terrestrial planet formation began by the condensation of small refractory dust particles, but observations with telescopes have not provided temporal resolution necessary to probe the timing of this stage. Our current understanding of the chronology of the first formation of solids in the solar protoplanetary disk is largely based on the short-lived ^{26}Al - ^{26}Mg systematics ($t_{1/2} = 0.72$ Ma) in refractory Ca-Al-rich inclusions (CAIs), the oldest datable solar system solids with an absolute U-corrected ^{207}Pb - ^{206}Pb age of 4.567 billion years (6, 7), found in chondritic meteorites. The use of ^{26}Al as a chronometer requires that this radionuclide be homogeneously distributed in the CAI-forming region(s). Since the discovery of ^{26}Al in 1976 (8), it has been established by numerous studies, especially high-precision in situ and bulk-inclusion analyses in the past 15 years, that large (>5 mm) CAIs in CV3 chondrites are characterized by well-constrained ^{26}Al - ^{26}Mg isochrons with slopes corresponding to $^{26}\text{Al}/^{27}\text{Al}$ of $5.2 (\pm 0.1) \times$

10^{-5} , and intercepts suggesting that the initial (pre- ^{26}Al decay) $^{26}\text{Mg}/^{24}\text{Mg}$ ratio ($\equiv \Delta^{26}\text{Mg}_0^*$; see the Supplementary Materials) of CAIs varies from -0.13 to -0.014% relative to a terrestrial standard value (9–15). It is noteworthy that in situ measurements are, in general, more sensitive to subsequent thermal reprocessing that disturbed the original magnesium isotopes than are bulk-inclusion analyses and, therefore, provide more information about the timing of the last melting/disturbance event and isotope reequilibration [interested readers are referred to (16) for more detailed discussions]. The fact that bulk-sample and some in situ work yielded $^{26}\text{Al}/^{27}\text{Al}$ of $5.2 (\pm 0.1) \times 10^{-5}$ but variable $\Delta^{26}\text{Mg}_0^*$ implies a <30,000-year time scale (inferred from the analytical error of $^{26}\text{Al}/^{27}\text{Al}$) for the formation of large CAIs in a reservoir with uniformly distributed ^{26}Al at this abundance level but slightly heterogeneous initial $^{26}\text{Mg}/^{24}\text{Mg}$. However, these centimeter-sized CAIs in CV3 chondrites, despite their primitiveness and early formation inferred from short- and long-lived radionuclides, are thought to have formed by melting and agglomeration of smaller particles (<10 μm) that condensed directly from the nebular gas. This fact calls into question how representative the value of $^{26}\text{Al}/^{27}\text{Al} = 5.2 (\pm 0.1) \times 10^{-5}$ recorded by these large CAIs is of the true initial ^{26}Al abundance and distribution in the protoplanetary disk. Here, we focus on the magnesium isotopic compositions of small refractory inclusions (mostly 30 to 50 μm in size), which are best understood as products of initial coagulation of high-temperature dust condensates (17). The aims of this study were to evaluate the ^{26}Al abundance and distribution during this time period and then to infer the chronologies of these small inclusions relative to those of the large CAIs in CV3 chondrites that have been the focus of many studies.

Previous efforts to understand the $^{26}\text{Al}/^{27}\text{Al}$ ratios in small refractory inclusions were mostly focused on SIMS (secondary ion mass spectrometry) analyses of individual 20- to 80- μm hibonite-rich ($\text{CaMg}_x\text{Ti}_x\text{Al}_{12-2x}\text{O}_{19}$) grains, corundum-bearing (Al_2O_3) inclusions, and grossite-bearing (CaAl_4O_7) inclusions primarily separated from the carbonaceous chondritic meteorites and of <10 μm corundum-rich grains extracted from carbonaceous and ordinary chondrites (18–28). According to equilibrium thermodynamics, these phases are predicted to be the first minerals directly condensing from a cooling gas of solar composition at ~ 1650 K at 10^{-3} bar (28). The inferred $^{26}\text{Al}/^{27}\text{Al}$ ratios in CM hibonite-rich samples are strongly correlated with mineralogy and morphology. Spinel-hibonite spherules (SHIBs) are characterized by an apparent scatter in $^{26}\text{Al}/^{27}\text{Al}$ from $\sim 6 \times 10^{-6}$ to 6×10^{-5} (18–22, 29). A statistical treatment of the data has revealed a major peak

Copyright © 2019
The Authors, some
rights reserved;
exclusive licensee
American Association
for the Advancement
of Science. No claim to
original U.S. Government
Works. Distributed
under a Creative
Commons Attribution
NonCommercial
License 4.0 (CC BY-NC).

¹Department of Earth, Planetary, and Space Sciences, University of California, Los Angeles, Los Angeles, CA 90095, USA. ²Lunar and Planetary Institute, 3600 Bay Area Boulevard, Houston, TX 77058, USA. ³NASA Johnson Space Center, 2101 NASA Parkway, Houston, TX 77058, USA. ⁴Department of Earth and Planetary Sciences, MSC03-2040, University of New Mexico, Albuquerque, NM 87131, USA. *Corresponding author. Email: mcliu@ucla.edu

at 4.9×10^{-5} , two secondary peaks at 3.5×10^{-5} and 6.5×10^{-6} , and two marginally resolved peaks at 6×10^{-5} and 2.5×10^{-5} (gray curve in Fig. 1) (21, 22). In contrast, monomineralic platy-hibonite crystals (PLACs) lack resolvable ^{26}Mg excesses that can be attributed to ^{26}Al decay, but instead show small variations of $\Delta^{26}\text{Mg}^*$ (deviation from a mass-dependent fractionation line; see Materials and Methods) between -4 and $+5\%$, which do not appear to be correlated with Al/Mg of the crystals. The ^{26}Al abundances deduced from corundum- and grossite-rich inclusions are broadly bimodal and do not correlate with mineral chemistry or textures. The two main peaks, composed of >50 and $\sim 40\%$ of measured corundum grains, respectively, are found at $^{26}\text{Al}/^{27}\text{Al} < 2 \times 10^{-6}$ and $^{26}\text{Al}/^{27}\text{Al} = (4 \text{ to } 5) \times 10^{-5}$ (23–26, 28); an intermediate ratio [$^{26}\text{Al}/^{27}\text{Al} = (1.0 \pm 0.1) \times 10^{-5}$] has recently been reported (28) and was included in the gray probability density curve in Fig. 1.

The meaning of the $^{26}\text{Al}/^{27}\text{Al}$ spread seen in hibonite-, corundum-, and grossite-rich inclusions still remains enigmatic. While isotopic resetting or late formation would be the most straightforward explanation for inclusions with $^{26}\text{Al}/^{27}\text{Al} < 5.2 \times 10^{-5}$, the possibility that these

objects formed prior to homogenization of $^{26}\text{Al}/^{27}\text{Al}$ to the value of 5.2×10^{-5} in the solar nebula has also been considered (21, 24, 25). If the latter is true, no constraints on formation time scales could be quantitatively derived for such grains. However, it should be noted that the SIMS primary ion beam used in previous studies was too large (~ 30 to $40 \mu\text{m}$) to permit multiple-spot analyses on single hibonite (in most cases) and corundum grains. Therefore, each measurement was analogous to “bulk” analysis, and the $^{26}\text{Al}/^{27}\text{Al}$ ratios were inferred via “model isochrons,” that is, connecting a data point to the assumed origin defined as $^{27}\text{Al}/^{24}\text{Mg} = 0$ and $^{26}\text{Mg}/^{24}\text{Mg} = 0.13932$ (the assumed terrestrial value) (30). This method, however, is only valid if two requirements were met. First, all corundum and hibonite must condense with the terrestrial $^{26}\text{Mg}/^{24}\text{Mg}$ ratio. However, the PLAC data, which suggested large $^{26}\text{Mg}/^{24}\text{Mg}$ heterogeneity ($\sim 10\%$) relative to the chondritic abundance in the early solar nebula (21, 31), have rendered this assumption questionable, especially if low $^{26}\text{Al}/^{27}\text{Al}$ was attributed to early formation. Second, these inclusions must have escaped any open-system magnesium isotope exchange with an external reservoir (e.g., solar nebula) after their formation, but this assumption has never been proven with certainty. Internal mineral isochrons in the earliest-formed solids are needed to infer assumption-free $^{26}\text{Al}/^{27}\text{Al}$ for a better understanding of the meaning of the $^{26}\text{Al}/^{27}\text{Al}$ ratio distribution.

As of now, only a handful of internal ^{26}Al isochrons have been obtained for hibonite-rich inclusions (including SHIBs, corundum-bearing hibonite, and grossite-hibonite-bearing CAIs) larger than $70 \mu\text{m}$ (22, 25, 26, 28). Overall the results corroborated those seen in the model isochron data. Most of the inferred $^{26}\text{Al}/^{27}\text{Al}$ ratios cluster at 4.8×10^{-5} , falling right on the major distribution peak at 4.9×10^{-5} (21). The intercepts of these internal isochrons were chondritic ($\Delta^{26}\text{Mg}_0^* = 0\%$) within analytical errors, indicating no resolvable initial $^{26}\text{Mg}/^{24}\text{Mg}$ heterogeneity. Lower $^{26}\text{Al}/^{27}\text{Al}$ ratios, broadly consistent with 3.5×10^{-5} and 2.5×10^{-5} , were also revealed, but no constraints on the associated intercept were obtained, except for one spinel-hibonite-rich sample in a recent study [$\Delta^{26}\text{Mg}_0^* = 0.8 \pm 0.2\%$, derived through weighted regression (22)], as the isochrons were forced through the assumed origin (see above). Therefore, how the $^{26}\text{Al}/^{27}\text{Al}$ variability seen in those potentially early formed solids relates to $^{26}\text{Al}/^{27}\text{Al} = 5.2 \times 10^{-5}$ recorded in large CAIs (early formation versus late formation) cannot be properly evaluated. To minimize the potential effects of any parent-body alteration, we chose small refractory inclusions, most of which are hibonite rich and have similar mineralogy to those in CM2 chondrites, found in a thin section of the CO3.0 chondrite Allan Hills (ALH) A77307, one of the most pristine meteorites known (32). We have analyzed 22 CAIs (~ 30 to $100 \mu\text{m}$ in size) using the University of California, Los Angeles (UCLA) CAMECA ims-1290 ion microprobe to infer ^{26}Al abundances through high-precision internal isochrons in the hope of better understanding the implications of $^{26}\text{Al}/^{27}\text{Al}$ variations in the context of early solar system chronology.

RESULTS

A positive correlation between the excesses of radiogenic ^{26}Mg ($\equiv^{26}\text{Mg}^*$) and $^{27}\text{Al}/^{24}\text{Mg}$ ratios was found within 18 individual inclusions, indicating in situ decay of ^{26}Al (fig. S1). The inferred $^{26}\text{Al}/^{27}\text{Al}$ ratios, calculated from bivariate error-weighted least squares regression by using the algorithm of (33), span a range from $8 (\pm 16.5) \times 10^{-6}$ to $5.73 (\pm 1.20) \times 10^{-5}$ (2σ errors), and the probability density

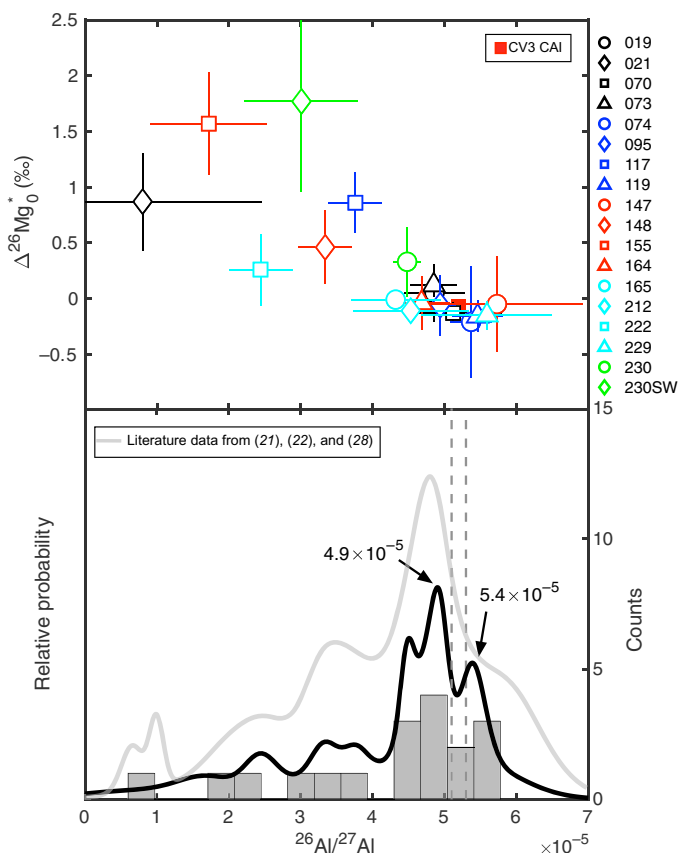


Fig. 1. Distribution of $^{26}\text{Al}/^{27}\text{Al}$ in 18 ALHA77307 CAIs. (Top) Inferred $^{26}\text{Al}/^{27}\text{Al}$ ratios are plotted against the associated $\Delta^{26}\text{Mg}_0^*$ (errors 2σ) obtained from the isochron plots. Each symbol indicates one inclusion. The solid red square represents $^{26}\text{Al}/^{27}\text{Al} = (5.2 \pm 0.1) \times 10^{-5}$ and $\Delta^{26}\text{Mg}_0^* = (-0.13 \text{ to } -0.014\%)$ inferred from large CV3 CAIs (using both bulk-sample and internal isochron methods). (Bottom) Black solid curve stands for the probability density plot calculated on the basis of the $^{26}\text{Al}/^{27}\text{Al}$ ratios acquired in this study. The probability curve based on the data of bulk and internal isochron-derived $^{26}\text{Al}/^{27}\text{Al}$ from CM SHIBs and one hibonite-grossite-rich inclusion (gray curve) is shown for comparison. The band formed by two gray dashed lines represents $^{26}\text{Al}/^{27}\text{Al} = (5.2 \pm 0.1) \times 10^{-5}$.

distribution is in excellent agreement with that calculated with the SHIB ^{26}Al abundances calculated by using model and internal isochrons [Fig. 1 and Table 1; model isochron data from (21) and internal isochron data from (22) and (28)]. The most prominent peak, which falls on $^{26}\text{Al}/^{27}\text{Al} = 4.9 \times 10^{-5}$, is identical to the major 4.9×10^{-5} peak in SHIBs. Multiple grains form a well-resolved peak at $^{26}\text{Al}/^{27}\text{Al} = 5.4 \times 10^{-5}$. This group and the SHIBs that constitute the marginally revealed 6.0×10^{-5} peak very likely belong to the same population, but the new data acquired here offer better resolution. The appearance of a small hump at $^{26}\text{Al}/^{27}\text{Al} = 4.5 \times 10^{-5}$ mainly arises from the small error on the inferred $^{26}\text{Al}/^{27}\text{Al}$ ratio for CAI 230, but the associated $\Delta^{26}\text{Mg}_0^* = 0.33 \pm 0.31\%$ suggests late isotopic closure, a result of either late formation or isotopic disturbance (see below). The same argument can be applied to two other minor peaks seen at lower $^{26}\text{Al}/^{27}\text{Al}$ ratios ($\sim 3.5 \times 10^{-5}$ and $\sim 2.5 \times 10^{-5}$), albeit very limited numbers of samples under each peak, because of the positive $\Delta^{26}\text{Mg}_0^*$ values associated with the samples.

Five CAIs (070, 074, 119, 147, and 229), which can be characterized by $^{26}\text{Al}/^{27}\text{Al} = 5.2 \times 10^{-5}$ within errors, all have a well-defined isochron (reduced $\chi^2 < 2$; fig. S1). A weighted least squares fit through the data points from the five inclusions together yields a slope corresponding to $^{26}\text{Al}/^{27}\text{Al} = 5.40 (\pm 0.13) \times 10^{-5}$ and an intercept of $(-0.14 \pm 0.03\%)$ as the initial $\Delta^{26}\text{Mg}_0^*$ (reduced $\chi^2 = 1.1$; Fig. 2A).

Table 1. Inferred $^{26}\text{Al}/^{27}\text{Al}$ ratios, initial $\Delta^{26}\text{Mg}_0^*$, and goodness of fit for 18 ^{26}Al -bearing ALHA77307 CAIs. Uncertainties are 2σ . hib, hibonite; pv, perovskite; sp, spinel; mel, melilitite; di, diopside rim; and fo, forsteritic olivine.

Sample	Minerals	$^{26}\text{Al}/^{27}\text{Al}$ ($\pm 2\sigma$)	$^{26}\text{Mg}_0^*$ (‰, $\pm 2\sigma$)	Reduced χ^2
019	hib	$(4.86 \pm 0.42) \times 10^{-5}$	0.05 ± 0.26	0.3
021	hib-pv-sp	$(0.80 \pm 1.65) \times 10^{-5}$	0.87 ± 0.44	2.0
070	sp-pv-di-ol	$(5.12 \pm 0.67) \times 10^{-5}$	-0.13 ± 0.09	0.7
073	hib-pv-sp	$(4.85 \pm 0.32) \times 10^{-5}$	0.12 ± 0.10	10
074	hib-pv-sp	$(5.37 \pm 0.29) \times 10^{-5}$	-0.21 ± 0.50	1.9
095	hib-sp	$(4.94 \pm 0.21) \times 10^{-5}$	-0.06 ± 0.27	1.0
117	hib-pv-sp-di	$(3.76 \pm 0.37) \times 10^{-5}$	0.86 ± 0.27	6.7
119	hib-pv-sp-di	$(5.46 \pm 0.35) \times 10^{-5}$	-0.16 ± 0.14	0.4
147	hib-sp-di	$(5.73 \pm 1.20) \times 10^{-5}$	-0.05 ± 0.43	1.2
148	hib-sp-di	$(3.34 \pm 0.37) \times 10^{-5}$	0.46 ± 0.33	9.4
155	hib-sp	$(1.72 \pm 0.81) \times 10^{-5}$	1.57 ± 0.46	22.3
164	hib-sp-di	$(4.68 \pm 0.39) \times 10^{-5}$	-0.04 ± 0.24	1.8
165	sp-di-fo	$(4.32 \pm 0.62) \times 10^{-5}$	-0.01 ± 0.04	0.9
212	sp-pv-di	$(4.53 \pm 0.80) \times 10^{-5}$	-0.11 ± 0.11	0.4
222	hib-sp	$(2.44 \pm 0.44) \times 10^{-5}$	0.26 ± 0.32	0.2
229	sp-pv-mel-di-ol	$(5.59 \pm 0.91) \times 10^{-5}$	-0.15 ± 0.13	1.4
230	hib-pv-sp-mel	$(4.48 \pm 0.19) \times 10^{-5}$	0.33 ± 0.31	3.8
230SW	hib-pv-sp-mel	$(3.01 \pm 0.79) \times 10^{-5}$	1.77 ± 0.81	0.7

This inferred ^{26}Al abundance, which agrees perfectly with the 5.40×10^{-5} peak in the probability density distribution, is only marginally resolved from $5.2 (\pm 0.1) \times 10^{-5}$. Although the initial $\Delta^{26}\text{Mg}_0^* = (-0.14 \pm 0.03\%)$ is resolved from that inferred for pristine bulk CAIs ($\Delta^{26}\text{Mg}_0^* = -0.04\%$) (10), it is identical to the values ($\Delta^{26}\text{Mg}_0^* = -0.13\%$) derived for a couple of large CAIs by using mineral isochrons (14, 15). Inclusions (019, 073, 095, 164, 165, and 212) that contribute to forming the peak at 4.9×10^{-5} also define an isochron, albeit with some scatter at low $^{27}\text{Al}/^{24}\text{Mg}$ (reduced $\chi^2 = 4.3$), from which $^{26}\text{Al}/^{27}\text{Al} = 4.89 (\pm 0.10) \times 10^{-5}$ and $\Delta^{26}\text{Mg}_0^* = (-0.04 \pm 0.03\%)$ can be inferred (Fig. 2B). CAIs 117, 148, 155, 222, 230, and 230SW are found to have much lower, yet nonzero,

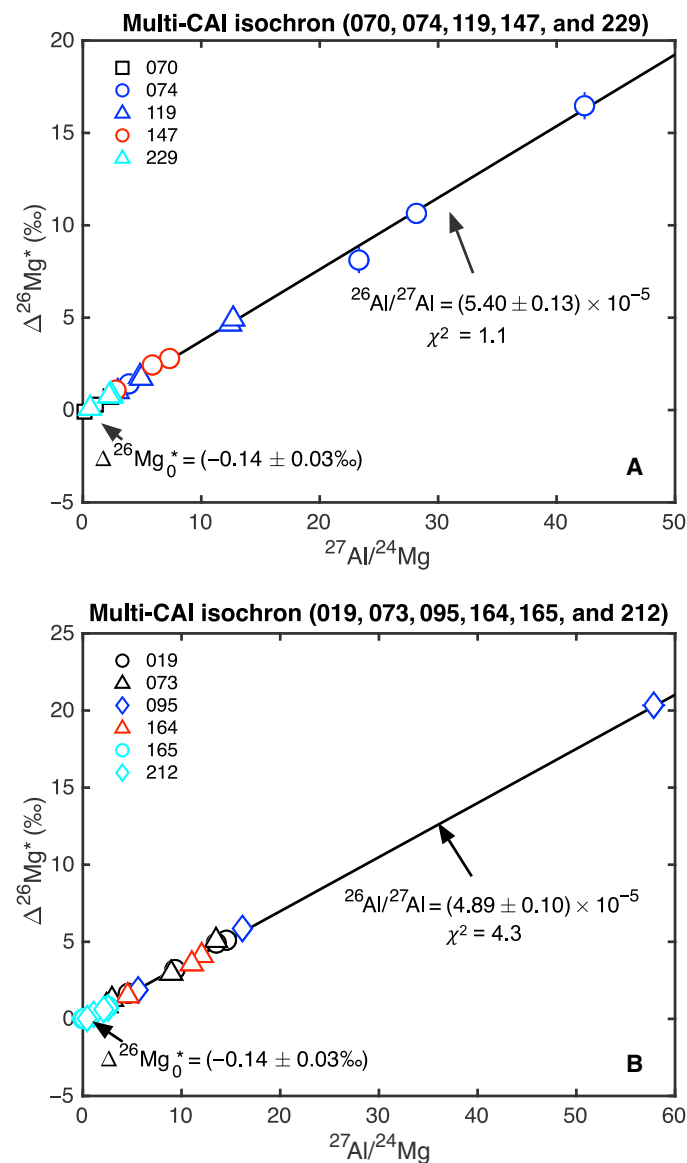


Fig. 2. Multi-CAI isochrons. (A) Five CAIs that make up the 5.4×10^{-5} peak in the probability density plot (Fig. 1) form a well-defined isochron ($\chi^2 = 1.1$), the slope of which corresponds to $^{26}\text{Al}/^{27}\text{Al} = (5.40 \pm 0.13) \times 10^{-5}$. (B) Six CAIs under the 4.9×10^{-5} peak are characterized by tightly constrained $^{26}\text{Al}/^{27}\text{Al} = (4.89 \pm 0.10) \times 10^{-5}$, albeit with some scatter ($\chi^2 = 4.3$). The intercept is broadly consistent with the chondritic value within errors. All errors are 2σ .

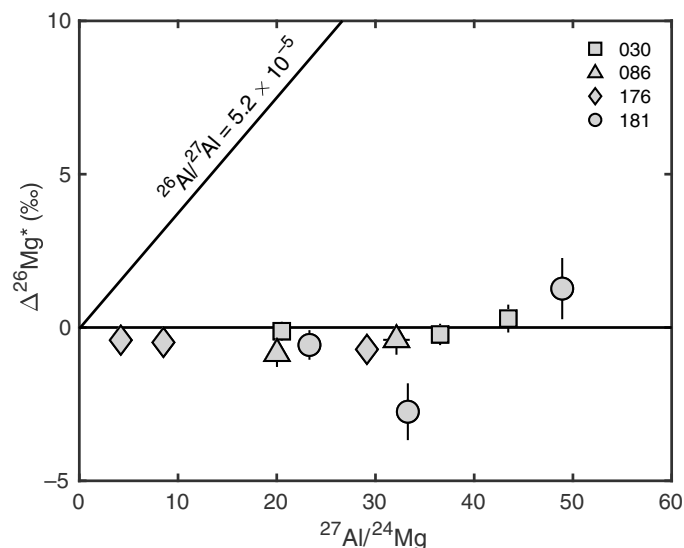


Fig. 3. CAIs devoid of resolved excesses in ^{26}Mg that could be attributed to the decay of ^{26}Al . Instead, $\Delta^{26}\text{Mg}^*$ appears to be slightly heterogeneous even within a single grain. A line corresponding to $^{26}\text{Al}/^{27}\text{Al} = 5.2 \times 10^{-5}$ is shown for reference. All errors are 2σ .

$^{26}\text{Al}/^{27}\text{Al}$ ratios and more positive $^{26}\text{Mg}_0^*$ compared with those in the two main populations, and the first three show apparent scatter along the best fit line (indicated by the reduced χ^2 values). CAI 021 is characterized by an isochron slope corresponding to $^{26}\text{Al}/^{27}\text{Al} = (8 \pm 16.5) \times 10^{-6}$ associated with $\Delta^{26}\text{Mg}_0^* = (0.87 \pm 0.44\%)$, suggesting that isotopic resetting took place after ^{26}Al had substantially decayed.

Four samples (030, 086, 176, and 181), either monomineralic hibonite or hibonite-corundum inclusions, lack resolvable excesses in radiogenic ^{26}Mg . Rather, their $\Delta^{26}\text{Mg}^*$ values range from -3 to $+1\%$ and are not correlated with $^{27}\text{Al}/^{24}\text{Mg}$ (Fig. 3), similar to what has been found in CM-chondrite PLACs (21, 31) and a couple of hibonite-bearing microspherules from in other CO3 chondrites (34).

DISCUSSION

The $^{26}\text{Al}/^{27}\text{Al}$ variation in small CO3.0 CAIs

Our new “assumption-free” ^{26}Al data from small CAIs in ALHA77307 (CO3.0) show two main populations of inclusions with regard to the inferred $^{26}\text{Al}/^{27}\text{Al}$ ratios and $\Delta^{26}\text{Mg}_0^*$. One group appears to have formed with $^{26}\text{Al}/^{27}\text{Al} = 5.40 (\pm 0.13) \times 10^{-5}$ and initial $\Delta^{26}\text{Mg}_0^* = (-0.14 \pm 0.03\%)$, whereas the other group is characterized by $^{26}\text{Al}/^{27}\text{Al} = 4.89 (\pm 0.10) \times 10^{-5}$ and the chondritic $\Delta^{26}\text{Mg}_0^*$ value of $(-0.04 \pm 0.03\%)$. This level of ^{26}Al abundance has been found, albeit with poor analytical precision, in three relatively larger CAIs (300 to 400 μm) in ALHA77307 from a previous study (34). Inclusions having $^{26}\text{Al}/^{27}\text{Al}$ lower than 4×10^{-5} are associated with more positive $\Delta^{26}\text{Mg}_0^*$ (up to 1.8%) and make up two small peaks at 3.5×10^{-5} and 2.5×10^{-5} . Such an $^{26}\text{Al}/^{27}\text{Al}-\Delta^{26}\text{Mg}_0^*$ relationship can be best understood in the context of postformation thermal processing, similar to that suggested to account for the $^{26}\text{Al}/^{27}\text{Al}$ differences between pristine (unmelted) and thermally reprocessed (igneous) CV3 CAIs [e.g., (35, 13, 36, 16)]. Therefore, inclusions having $^{26}\text{Al}/^{27}\text{Al} = 5.4 \times 10^{-5}$ and $\Delta^{26}\text{Mg}_0^* = -0.14\%$ could be considered the most pristine among those analyzed here and should most faithfully record the isotopic signatures of the formation region. These two values are in good agreement with the esti-

mates for “true” solar system $^{26}\text{Al}/^{27}\text{Al} = (5.62 \pm 0.42) \times 10^{-5}$ and $\Delta^{26}\text{Mg}_{0,i}^* = -(0.052 \pm 0.013\%)$ based on CV CAI data (16). The peaks at lower $^{26}\text{Al}/^{27}\text{Al}$ (along with more positive $\Delta^{26}\text{Mg}_0^*$) would have been a consequence of late thermal processing of these early formed inclusions that had led to (partial) isotopic reequilibration. The major thermal event appears to have occurred to reset the majority of the inclusions when $^{26}\text{Al}/^{27}\text{Al} = 4.9 \times 10^{-5}$, i.e., $\sim 10^5$ years after initial formation. Support for reprocessing of small CAIs at this time can be derived from the fact that average $^{27}\text{Al}/^{24}\text{Mg} = 2.8$, a ratio that would have only existed in a reservoir composed primarily of refractory solids [a gas reservoir would have average solar $^{27}\text{Al}/^{24}\text{Mg} \sim 0.101$ (37)], would be required to change $\Delta^{26}\text{Mg}_0^*$ from -0.14% to -0.04% by the decay of ^{26}Al from $^{26}\text{Al}/^{27}\text{Al} = 5.4 \times 10^{-5}$ to 4.9×10^{-5} . It is noteworthy that this $^{26}\text{Al}/^{27}\text{Al}$ value of 4.9×10^{-5} has been registered not only by the CO3 inclusions but also by many CM2 SHIBs, CV3 CAIs, and corundum grains [e.g., (13, 15, 21, 22, 24)], implying that such thermal processing was widespread in the regions where refractory inclusions resided or formed.

There could have been additional thermal events that reset existing solids hundreds of thousands of years after the major one at $^{26}\text{Al}/^{27}\text{Al} = 4.9 \times 10^{-5}$, as indicated by the low $^{26}\text{Al}/^{27}\text{Al}$, but positive $\Delta^{26}\text{Mg}_0^*$, values of CAIs 021, 117, 148, 155, 222, 230, and 230SW. The following discussion about these CAIs is based on the approach used in previous work (13, 16); more details can be found in these references. All inclusions except 155 are characterized by slightly negative mass-dependent isotope fractionation ($\delta^{25}\text{Mg} = -1$ to -4% ; table S1), indicating that they have a condensation origin and most likely have not experienced any evaporation processes. Therefore, we argue that these CAIs obtained their current chemical compositions during initial condensation, and thermal reprocessing did not further fractionate Al/Mg of the inclusions. Consequently, the present-day $^{27}\text{Al}/^{24}\text{Mg}$ and inferred $^{26}\text{Al}/^{27}\text{Al}$ of CAIs could be used to back-calculate the true initial $^{26}\text{Mg}/^{24}\text{Mg}$ (denoted $\Delta^{26}\text{Mg}_{0,i}^*$ to avoid confusion with isochron-derived $\Delta^{26}\text{Mg}_0^*$) they formed with. As can be seen in Fig. 4, the $\Delta^{26}\text{Mg}_{0,i}^*$ values for CAIs 021, 117, 148, 222, 230, and 230SW appear to show a range when $^{26}\text{Al}/^{27}\text{Al} = 5.4 \times 10^{-5}$, but most of them cluster at $\sim -0.4\%$ with a full width at half maximum ($\sim 2.3\sigma$) of $\pm 0.3\%$, broadly consistent with -0.14% within errors. This means that these inclusions could still have formed together with those constituting the $^{26}\text{Al}/^{27}\text{Al} = 5.4 \times 10^{-5}$ peak. It should be noted that given the limited number of data points used in this exercise and analytical errors associated with the measured $\Delta^{26}\text{Mg}_0^*$ and $^{27}\text{Al}/^{24}\text{Mg}$ for these inclusions, the individual back-calculated $\Delta^{26}\text{Mg}_{0,i}^*$ values would also have nonnegligible uncertainties, and thus, the true range of magnesium heterogeneity at this time cannot be precisely constrained. More work is needed.

CAI 155 appears to have a different evolution history from the others due to its slightly positive $\delta^{25}\text{Mg}$ ($\sim 3\%$; table S1). This level of isotope fractionation suggests that $\sim 20\%$ of the initial magnesium was lost from this CAI by evaporation before the final formation (38). Therefore, the present-day $^{27}\text{Al}/^{24}\text{Mg}$ of CAI 155 did not originate from the initial condensation and thus cannot be used to infer $\Delta^{26}\text{Mg}_{0,i}^*$. Although it could be possible to constrain the evolution history by calculating the possible bulk $^{27}\text{Al}/^{24}\text{Mg}$ for the preevaporation CAI, the highly disturbed magnesium isotopic composition would make this a possible overinterpretation of data.

The above discussion of the $^{26}\text{Al}/^{27}\text{Al}-\Delta^{26}\text{Mg}_0^*$ relationship is based on reprocessing of inclusions that have formed early at $^{26}\text{Al}/^{27}\text{Al} = 5.4 \times 10^{-5}$. While the samples characterized by $^{26}\text{Al}/^{27}\text{Al} < 4 \times 10^{-5}$ are

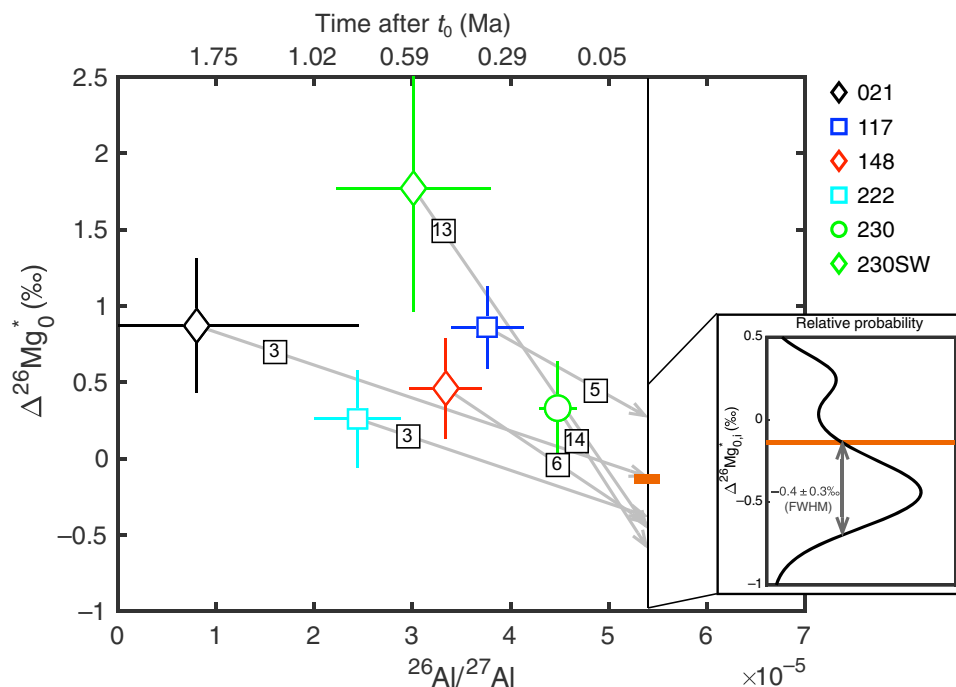


Fig. 4. The true initial $^{26}\text{Mg}/^{24}\text{Mg}$ ($\equiv \Delta^{26}\text{Mg}_{0,i}^*$) of individual CAI, calculated from isochron-derived $^{26}\text{Al}/^{27}\text{Al}$ and $\Delta^{26}\text{Mg}_{0,i}^*$, and bulk $^{27}\text{Al}/^{24}\text{Mg}$ estimated by using scanning electron microscopy–energy-dispersive x-ray spectroscopy. A gray arrow is drawn from each CAI data point to the $^{26}\text{Al}/^{27}\text{Al}$ ratio of 5.4×10^{-5} (defined as “ t_0 ,” the vertical solid line), with the slope determined from the CAI’s present-day bulk $^{27}\text{Al}/^{24}\text{Mg}$, which is the number shown in a black square. The small orange rectangle stands for $^{26}\text{Al}/^{27}\text{Al} = (5.40 \pm 0.13) \times 10^{-5}$ and $\Delta^{26}\text{Mg}_{0,i}^* = (-0.14 \pm 0.03)\text{‰}$. (Inset) A blow-up of the area where arrows intersect the vertical solid line, showing the distribution of back-calculated $\Delta^{26}\text{Mg}_{0,i}^*$ in the form of a probability density plot. The horizontal orange bar represents $\Delta^{26}\text{Mg}_{0,i}^* = (-0.14 \pm 0.03)\text{‰}$. Most of the values cluster at $\Delta^{26}\text{Mg}_{0,i}^* = -0.4\text{‰}$ with a full width at half maximum (FWHM) ($\sim 2.3\sigma$) of $\pm 0.3\text{‰}$.

still best explained in this context (except CAI 155), those making up the peak at $^{26}\text{Al}/^{27}\text{Al} = 4.9 \times 10^{-5}$ (along with $\Delta^{26}\text{Mg}_{0,i}^* = -0.04\text{‰}$) may be understood in a different scenario. It is known from the literature data that $\Delta^{26}\text{Mg}_{0,i}^*$ in the CAI formation reservoir(s) appeared to be heterogeneous between -0.13 and -0.014‰ when $^{26}\text{Al}/^{27}\text{Al}$ was homogeneous at 5.2×10^{-5} , and could have varied even more at an earlier time (at $^{26}\text{Al}/^{27}\text{Al} = 5.4 \times 10^{-5}$; see above). To make $\Delta^{26}\text{Mg}_{0,i}^* = -0.04\text{‰}$ at $^{26}\text{Al}/^{27}\text{Al} = 4.9 \times 10^{-5}$ in a gas reservoir of solar composition ($^{27}\text{Al}/^{24}\text{Mg} = 0.101$), $\Delta^{26}\text{Mg}_{0,i}^*$ at $^{26}\text{Al}/^{27}\text{Al} = 5.4 \times 10^{-5}$ would have to be -0.044‰ , which is well within the range of variation. Therefore, it is conceivable a reservoir of such $\Delta^{26}\text{Mg}_{0,i}^*$, from which one generation of inclusions formed during the nebula-wide thermal event at $^{26}\text{Al}/^{27}\text{Al} = 4.9 \times 10^{-5}$, existed. With our current dataset, it is difficult to prove or disprove this explanation. One testable prediction is that there should exist other populations of inclusions characterized by $^{26}\text{Al}/^{27}\text{Al} = 4.9 \times 10^{-5}$ but with $\Delta^{26}\text{Mg}_{0,i}^*$ closer to -0.14‰ . More high-precision measurements of small CAIs should be able to shed more light on this issue.

There are still two more alternatives for the observed $^{26}\text{Al}/^{27}\text{Al}$ distribution, but we argue that neither of them can account for the $^{26}\text{Al}/^{27}\text{Al}$ – $\Delta^{26}\text{Mg}_{0,i}^*$ relationship. The first possibility is that these inclusions had formed prior to homogenization of ^{26}Al and registered the heterogeneities of ^{26}Al and Mg isotopes in the (inner) solar nebula (21). However, if this was true, one would expect a more random relationship between $^{26}\text{Al}/^{27}\text{Al}$ and $\Delta^{26}\text{Mg}_{0,i}^*$. Instead, we observe that lower inferred ^{26}Al abundances are always accompanied by more positive $\Delta^{26}\text{Mg}_{0,i}^*$. Therefore, the $^{26}\text{Al}/^{27}\text{Al}$ variation is unlikely to have originated from the ^{26}Al (and magnesium isotope) heterogeneities in the formation region(s) and implies that the early formation hy-

pothesis for SHIBs in a heterogeneous solar nebula based on the model isochron data [e.g., (21)] would be incorrect. The second possible scenario is that samples having lower $^{26}\text{Al}/^{27}\text{Al}$ would have formed with elevated $\Delta^{26}\text{Mg}_{0,i}^*$ from a reservoir in which ^{26}Al has partially decayed. One serious problem with this explanation is that multiple formation reservoirs in the solar nebula, characterized by different Al/Mg ratios, would be required to result in different $\Delta^{26}\text{Mg}_{0,i}^*$. For example, CAI 222 and CAI 230SW would have formed in a region where Al/Mg = ~ 1.5 and ~ 10 , respectively, $\sim 800,000$ and $\sim 600,000$ years after the inclusions with $^{26}\text{Al}/^{27}\text{Al} = 5.4 \times 10^{-5}$. Forming such reservoirs and keeping the required Al/Mg ratios in individual reservoirs for hundreds of thousands of years without being homogenized would be astrophysically difficult, if not impossible [e.g., (39)].

Timing and duration of dust formation and agglomeration

The well-defined distribution peak and multi-CAI isochron revealing $^{26}\text{Al}/^{27}\text{Al} = 5.40 (\pm 0.13) \times 10^{-5}$ (Figs. 1 and 2A), albeit only marginally resolved from the ratio of $5.2 (\pm 0.1) \times 10^{-5}$ characterizing pristine large CV3 CAIs, shed light on the timing and time scales of the first stage of dust formation in the solar nebula. These CO3 CAIs have irregular shapes and nodular structures (see the Supplementary Materials), which imply that they have never been melted since their formation, and their small sizes, varying from $\sim 30 \mu\text{m}$ (CAI 147) to $\sim 100 \mu\text{m}$ (CAI 229), suggest they represent products from early stages of coagulation of primitive high-temperature condensates directly from a nebular gas. Along with $^{26}\text{Al}/^{27}\text{Al} = 5.40 (\pm 0.13) \times 10^{-5}$, one could infer a time scale of less than 50,000 years (deduced from the error of $^{26}\text{Al}/^{27}\text{Al}$, which corresponds to $\pm 25,000$ years) for the formation of refractory inclusions

several tens of micrometers in size by accretion of micrometer-sized dust. Centimeter-sized CAIs would have started to emerge during the late period of this coagulation stage and formed in abundance ~40,000 years after the majority of the 30- to 100- μm -sized inclusions have appeared in the nebula. This time scale is consistent with that predicted by a recent astrophysical model, which couples CAI formation to the physics of material infall and disk building (40). $\Delta^{26}\text{Mg}_0^* = -0.14\%$ inferred for small CO3 CAIs, on the other hand, may not have too much chronological significance when compared with that of CV3 CAIs (-0.04%), because, as mentioned before, CV3 CAI data suggest that the solar nebula was characterized by slightly heterogeneous $\Delta^{26}\text{Mg}_0^*$, varying from -0.13 to -0.014% while $^{26}\text{Al}/^{27}\text{Al} = 5.2 \times 10^{-5}$ (12, 14, 15). It is therefore conceivable that condensation of micrometer-sized dust particles followed by rapid agglomeration first into 30- to 100- μm -sized CAIs (such as those studied here) and eventually into centimeter-sized ones all took place in a reservoir characterized by $\Delta^{26}\text{Mg}_0^* = -0.14\%$ within tens of thousands of years of solar system formation.

The short time scale inferred above for dust condensation and agglomeration also allows a more quantitative understanding of the chronology of refractory inclusions devoid of live ^{26}Al . Just as the PLACs from CM2 chondrites, ^{26}Al -free refractory inclusions also exist in CO3 chondrites (CAIs 030, 086, 176, and 181). CM PLACs have been interpreted, albeit very qualitatively, to have formed in an isotopically heterogeneous solar nebula, possibly before CAIs with $^{26}\text{Al}/^{27}\text{Al} = 5.2 \times 10^{-5}$, because they preserve large (up to 300‰) nucleosynthetic anomalies in neutron-rich isotopes ^{48}Ca and ^{50}Ti (21). Although these four inclusions were not measured for calcium and titanium isotopes here, previous related studies have revealed enrichments or deficits in $\delta^{48}\text{Ca}$ or $\delta^{50}\text{Ti}$ by up to 30‰ in other CO3 chondrite CAIs that show no evidence for incorporation of live ^{26}Al (34, 41). Therefore, based on the similarities in the range of $\Delta^{26}\text{Mg}_0^*$ variation and preservation of nucleosynthetic anomalies, the ^{26}Al -free CO3 CAIs may have formed close in time, if not contemporaneously, with CM PLACs. This would allow for the possibility that reservoirs that were ^{26}Al poor, yet highly heterogeneous in $\Delta^{26}\text{Mg}_0^* - \delta^{48}\text{Ca} - \delta^{50}\text{Ti}$, may have existed before well-homogenized reservoirs with $^{26}\text{Al}/^{27}\text{Al} = 5.4 \times 10^{-5}$. However, these reservoirs disappeared in less than 50,000 years, a limit set by the dust condensation and coagulation time scale (see above). This broadly agrees with the homogenization time ($<10^4$ years) by hydrodynamic mixing in a marginally gravitationally unstable disk (39). Finer temporal resolution could potentially be achieved if more small samples having $^{26}\text{Al}/^{27}\text{Al} = 5.4 \times 10^{-5}$ were found in the future.

Implications for evolution time scales of early solar system

The above interpretations that $^{26}\text{Al}/^{27}\text{Al}$ ratios of 5.4×10^{-5} and 4.9×10^{-5} have marked, respectively, the onset of dust formation in the protosolar nebula and the major thermal event affecting most already-formed CAIs also have important implications for the evolution time scales of the protosun. Theoretical modeling has shown that the temperature at the disk midplane would increase as material falls into it from the circumstellar envelope and reach the maximum at the cessation of infall. The timing of the latter coincides approximately with the transition from class I to class II stage of YSOs [e.g., (42)]. Therefore, isotopic resetting of most CAIs could have taken place when the inner-disk temperature was at its peak. This implies that $^{26}\text{Al}/^{27}\text{Al} = 4.9 \times 10^{-5}$ would have corresponded to the end of class I or the beginning of class II of the protosun. The 100,000-year time difference

calculated from the above two $^{26}\text{Al}/^{27}\text{Al}$ ratios is comparable to the mean life ($\sim 125,000$ years) of the class I stage of YSOs derived from observations of protostars in each evolutionary class (43) and could therefore represent the duration for the Sun being a class I source.

MATERIALS AND METHODS

Sample description

The CAIs in this study were found in situ on a polished thin section of ALHA77307 by using a FEI Quanta three-dimensional field emission gun scanning electron microscope/focused ion beam instrument fitted with an EDAX Apollo 40 SDD Energy Dispersive Spectroscopy system at the University of New Mexico. Of 22 samples analyzed, 18 were hibonite rich, and the rest were hibonite free, spinel rich, with sizes ranging from 10 to $\sim 100 \mu\text{m}$ (fig. S1). Most hibonite-rich inclusions consist of randomly oriented hibonite laths intergrown with or surrounded by spinel, often rimmed by diopside. However, three inclusions (019, 176, and 181) were spinel-free hibonite crystals. Corundum occurred with hibonite in two inclusions (030 and 086). Four hibonite-free inclusions (070, 165, 212, and 229) have nodular structures consisting of a spinel core surrounded by a diopside rim, often with thin layers of olivine on the exterior of the diopside rim. Fine-grained perovskite is a common accessory mineral in many inclusions, whereas melilite is a rare mineral occurring only in two inclusions (229 and 230). The shape and morphology of the samples suggest that they have not been melted since their initial formation by direct high-temperature condensation (17). More detailed descriptions about individual inclusions can be found in the Supplementary Materials.

Secondary ion mass spectrometry

In situ isotope analyses of ^{26}Al - ^{26}Mg were performed in three separate sessions on the CAMECA ims-1290 ion microprobe at UCLA by following a method described previously (44). The target inclusions on the polished meteorite thin section were bombarded with a 1- to 8-nA $^{16}\text{O}^-$ primary ion beam ($\phi \sim 1.5$ to $4 \mu\text{m}$) generated by a Hyperion-II oxygen plasma source, yielding Mg and Al secondary ion signals intense enough to be simultaneously measured with multiple Faraday cups without switching the magnetic field setting. Each spot analysis consisted of 45 s of “presputtering” and 300 s (10 s per cycle for 30 cycles) of data acquisition. Mass resolution ($M/\Delta M$) was set at 2500 (corresponding to exit slit #1 on the multicollection trolleys) to separate doubly charged interferences ($^{48}\text{Ca}^{2+}$ and $^{48}\text{Ti}^{2+}$) from $^{24}\text{Mg}^+$. $^{24}\text{MgH}^+$ cannot be fully resolved from $^{25}\text{Mg}^+$ under such mass resolution, but the vacuum condition in the analysis chamber (pressure $\leq 1 \times 10^{-9}$ torr) made the hydride contribution negligible ($<0.05\%$). A suite of terrestrial standards [Burma spinel, San Carlos (SC) olivine, San Carlos pyroxene, Madagascar hibonite, and isotopically normal synthetic glass of fassaite composition known as “P0”] were used to characterize instrumental mass fractionation (IMF) of magnesium isotopes during ion probe analyses. IMF is defined as

$$\alpha_i = \frac{(i\text{Mg}/^{24}\text{Mg})_m}{(i\text{Mg}/^{24}\text{Mg})_{\text{true}}}$$

where $i = 25$ or 26 , and m stands for “measured.” All these terrestrial standards were assumed to have the true magnesium isotopic compositions of $^{25}\text{Mg}/^{24}\text{Mg} = 0.12663$ and $^{26}\text{Mg}/^{24}\text{Mg} = 0.13932$ (30). α_{25} and

α_{26} would have the following relationship when using an exponential mass fractionation law

$$\alpha_{25} = (\alpha_{26})^\beta$$

β is the IMF factor. To derive this quantity, we first expressed the deviations of measured isotopic ratios from the assumed true values in modified delta notation as

$$\delta^i \text{Mg}' (\%) = \ln \alpha_i \times 1000$$

and then obtained the slope of linear regression through data points on Mg-rich standards (spinel, SC olivine, and SC pyroxene) in $\delta^{25}\text{Mg}'$ - $\delta^{26}\text{Mg}'$ space (fig. S2). The β value slightly varied between 0.510 and 0.516 from one session to another, but this range is comparable to those obtained on other ims-1200 series ion microprobe [e.g., (16, 21)]. The horizontal deviation from a mass fractionation line as a result of the decay of ^{26}Al ($\equiv \Delta^{26}\text{Mg}^*$) was calculated with the formula recommended in (45)

$$\Delta^{26}\text{Mg}^* = \delta^{26}\text{Mg} - \left[(1 + \delta^{25}\text{Mg}/1000)^{1/\beta} - 1 \right] \times 1000$$

where $\delta^{25,26}\text{Mg} = (\alpha_{25,26} - 1) \times 1000$. In this study, $\delta^i \text{Mg}$ and $\delta^i \text{Mg}'$ are almost identical within errors. A synthetic in-house glass of fassaite composition doped with a 10.3% excess in ^{26}Mg , referred to as P10, was measured to check the accuracy of the analysis (fig. S2). It should be pointed out that the calculated $\Delta^{26}\text{Mg}^*$ values depended very little on β . If the recommended $\beta = 0.5128$ was used (45), the difference in the resulting $\Delta^{26}\text{Mg}^*$ could not be resolved outside of reported uncertainties. The internal error (σ_{internal}) of $\Delta^{26}\text{Mg}^*$ for a spot analysis was the standard error of the mean (SEM) on a cycle-by-cycle basis, and the final reported error was calculated as

$$\sigma_{\text{final}} = \sqrt{\sigma_{\text{internal}}^2 + \sigma_{\text{external}}^2}$$

where σ_{external} is the SEM of repeated measurements on the corresponding standard.

Aluminum and magnesium ions have slightly different yields during ion probe analysis. Therefore, the relative sensitivity factor (RSF) of Al to Mg, defined as $(^{27}\text{Al}/^{24}\text{Mg})_{\text{true}} / (^{27}\text{Al}/^{24}\text{Mg})_{\text{m}}$, needs to be characterized for different mineral phases by using the corresponding standards with known $^{27}\text{Al}/^{24}\text{Mg}$ ratios. The true $^{27}\text{Al}/^{24}\text{Mg}$ ratios of measured CAI minerals, including Al-rich diopside, spinel, and hibonite were derived by applying the RSFs determined on P0 glass, Burma spinel, and Madagascar hibonite, respectively, in each session. Al/Mg ratios of CAI olivine were not corrected for RSF because (i) they were too low (~ 0.0086) to have any observable effects on the determination of isochron slope and (ii) the low aluminum concentration in San Carlos olivine did not allow for an accurate estimate of RSF. The RSF values and corresponding errors obtained in each session on each standard are listed in table S2.

SUPPLEMENTARY MATERIALS

Supplementary material for this article is available at <http://advances.sciencemag.org/cgi/content/full/5/9/eaaw3350/DC1>

Supplementary Materials and Methods

Fig. S1. Individual internal ^{26}Al isochrons obtained in 18 ^{26}Al -bearing inclusions.

Fig. S2. Example of IMF characterized in one analysis session.

Table S1. Magnesium isotopic compositions of 22 inclusions analyzed in this study.

Table S2. Relative sensitivity factors determined on standards with known $^{27}\text{Al}/^{24}\text{Mg}$ in three analysis sessions.

REFERENCES AND NOTES

- Blum, G. Wurm, The growth mechanisms of macroscopic bodies in protoplanetary disks. *Annu. Rev. Astron. Astrophys.* **46**, 21–56 (2008).
- J. P. Williams, L. A. Cieza, Protoplanetary disks and their evolution. *Annu. Rev. Astron. Astrophys.* **49**, 67–117 (2011).
- ALMA Partnership, C. L. Brogan, L. M. Pérez, T. R. Hunter, W. R. F. Dent, A. S. Hales, R. E. Hills, S. Corder, E. B. Fomalont, C. Vlahakis, Y. Asaki, D. Barkats, A. Hirota, J. A. Hodge, C. M. V. Impellizzeri, R. Kneissl, E. Liuzzo, R. Lucas, N. Marcelino, S. Matsushita, K. Nakanishi, N. Phillips, A. M. S. Richards, I. Toledo, R. Aladro, D. Brogiere, J. R. Cortes, P. C. Cortes, D. Espada, F. Galarza, D. Garcia-Appadoo, L. Guzman-Ramirez, E. M. Humphreys, T. Jung, S. Kamenoi, R. A. Laing, S. Leon, G. Marconi, A. Mignano, B. Nikolic, L.-A. Nyman, M. Radiszcz, A. Remijan, J. A. Rodón, T. Sawada, S. Takahashi, R. P. J. Tilanus, B. Villa Vilaro, L. C. Watson, T. Wiklund, E. Akiyama, E. Chapillon, I. de Gregorio-Monsalvo, J. Di Francesco, F. Gueth, A. Kawamura, C.-F. Lee, Q. Nguyen Luong, J. Mangum, V. Pietu, P. Sanhueza, K. Saigo, S. Takakuwa, C. Ubach, T. van Kempen, A. Wootten, A. Castro-Carrizo, H. Francke, J. Gallardo, J. Garcia, S. Gonzalez, T. Hill, T. Kaminski, Y. Kurono, H.-Y. Liu, C. Lopez, F. Morales, K. Plarre, G. Schieven, L. Testi, L. Videla, E. Villard, P. Andreani, J. E. Hibbard, K. Tatematsu, The 2014 ALMA long baseline campaign: first results from high angular resolution observations toward the HL Tau region. *Astrophys. J. Lett.* **808**, L3 (2015).
- C. Carrasco-González, T. Henning, C. J. Chandler, H. Linz, L. Pérez, L. F. Rodríguez, R. Galván-Madrid, G. Anglada, T. Birnstiel, R. van Boekel, M. Flock, H. Klahr, E. Macias, K. Menten, M. Osorio, L. Testi, J. M. Torrelles, Z. Zhu, The VLA view of the HL Tau disk: Disk mass, grain evolution, and early planet formation. *Astrophys. J. Lett.* **821**, L16 (2016).
- T. S. Kruijer, M. Touboul, M. Fischer-Gödde, K. R. Bermingham, R. J. Walker, T. Kleine, Protracted core formation and rapid accretion of protoplanets. *Science* **344**, 1150–1154 (2014).
- Y. Amelin, A. Kaltenbach, T. Izuka, C. H. Stirling, T. R. Ireland, M. Petaev, S. B. Jacobsen, U–Pb chronology of the Solar System's oldest solids with variable $^{238}\text{U}/^{235}\text{U}$. *Earth Planet. Sci. Lett.* **300**, 343–350 (2010).
- J. N. Connelly, M. Bizzarro, A. N. Krot, Å. Nordlund, D. Wielandt, M. A. Ivanova, The absolute chronology and thermal processing of solids in the solar protoplanetary disk. *Science* **338**, 651–655 (2012).
- T. Lee, D. A. Papanastassiou, G. J. Wasserburg, Demonstration of ^{26}Mg excess in Allende and evidence for ^{26}Al . *Geophys. Res. Lett.* **3**, 41–44 (1976).
- M. Bizzarro, J. A. Baker, H. Haack, Mg isotope evidence for contemporaneous formation of chondrules and refractory inclusions. *Nature* **431**, 275–278 (2004).
- B. Jacobsen, Q.-Z. Yin, F. Moynier, Y. Amelin, A. N. Krot, K. Nagashima, I. D. Hutcheon, H. Palme, ^{26}Al - ^{26}Mg and ^{207}Pb - ^{206}Pb systematics of Allende CAIs: Canonical solar initial $^{26}\text{Al}/^{27}\text{Al}$ ratio reinstated. *Earth Planet. Sci. Lett.* **272**, 353–364 (2008).
- G. J. MacPherson, E. S. Bullock, P. E. Janney, N. T. Kita, T. Ushikubo, A. M. Davis, M. Wadhwa, A. N. Krot, Early solar nebula condensates with canonical, not supracanonical, INITIAL $^{26}\text{Al}/^{27}\text{Al}$ ratios. *Astrophys. J.* **711**, L117–L121 (2010).
- K. K. Larsen, A. Trinquier, C. Paton, M. Schiller, D. Wielandt, M. A. Ivanova, J. N. Connelly, Å. Nordlund, A. N. Krot, M. Bizzarro, Evidence for magnesium isotope heterogeneity in the solar protoplanetary disk. *Astrophys. J.* **735**, L37–L43 (2011).
- G. J. MacPherson, N. T. Kita, T. Ushikubo, E. S. Bullock, A. M. Davis, Well-resolved variations in the formation ages for Ca–Al-rich inclusions in the early Solar System. *Earth Planet. Sci. Lett.* **331–332**, 43–54 (2012).
- G. J. Wasserburg, J. Wimpenny, Q.-Z. Yin, Mg isotopic heterogeneity, Al–Mg isochrons, and canonical $^{26}\text{Al}/^{27}\text{Al}$ in the early solar system. *Meteorit. Planet. Sci.* **47**, 1980–1997 (2012).
- G. J. MacPherson, E. S. Bullock, T. J. Jenner, D. Nakashima, N. T. Kita, M. A. Ivanova, A. N. Krot, M. I. Petaev, S. B. Jacobsen, High precision Al–Mg systematics of forsterite-bearing Type B CAIs from CV3 chondrites. *Geochim. Cosmochim. Acta* **201**, 65–82 (2017).
- R. K. Mishra, M. Chaussidon, Timing and extent of Mg and Al isotopic homogenization in the early inner Solar System. *Earth Planet. Sci. Lett.* **390**, 318–326 (2014).
- J. Han, A. J. Brearley, Microstructures and formation history of millite-rite calcium–aluminum-rich inclusions from the ALHA77307 CO3.0 chondrite. *Geochim. Cosmochim. Acta* **201**, 136–154 (2017).
- A. J. Fahey, J. N. Goswami, K. D. McKeegan, E. Zinner, ^{26}Al , ^{244}Pu , ^{50}Ti , REE, and trace element abundances in hibonite grains from CM and CV meteorites. *Geochim. Cosmochim. Acta* **51**, 329–350 (1987).
- T. R. Ireland, Correlated morphological, chemical, and isotopic characteristics of hibonites from the Murchison carbonaceous chondrite. *Geochim. Cosmochim. Acta* **52**, 2827–2839 (1988).
- S. Sahijpal, J. N. Goswami, A. M. Davis, L. Grossman, R. S. Lewis, A stellar origin for the short-lived nuclides in the early Solar System. *Nature* **391**, 559–561 (1998).

21. M.-C. Liu, M. Chaussidon, C. Göpel, T. Lee, A heterogeneous solar nebula as sampled by CM hibonite grains. *Earth Planet. Sci. Lett.* **327–328**, 75–83 (2012).
22. L. Kööp, D. Nakashima, P. R. Heck, N. T. Kita, T. J. Tenner, A. N. Krot, K. Nagashima, C. Park, A. M. Davis, New constraints on the relationship between ^{26}Al and oxygen, calcium, and titanium isotopic variation in the early Solar System from a multielement isotopic study of spinel-hibonite inclusions. *Geochim. Cosmochim. Acta* **184**, 151–172 (2016).
23. A. Virag, E. Zinner, S. Amari, E. Anders, An ion microprobe study of corundum in the Murchison meteorite: Implications for ^{26}Al and ^{16}O in the early solar system. *Geochim. Cosmochim. Acta* **55**, 2045–2062 (1991).
24. K. Makide, K. Nagashima, A. N. Krot, G. R. Huss, F. J. Ciesla, E. Hellebrand, E. Gaidos, L. Yang, Heterogeneous distribution of ^{26}Al at the birth of the solar system. *Astrophys. J.* **733**, L31–L34 (2011).
25. K. Makide, K. Nagashima, A. N. Krot, G. R. Huss, I. D. Hutcheon, E. Hellebrand, M. I. Petaev, Heterogeneous distribution of ^{26}Al at the birth of the Solar System: Evidence from corundum-bearing refractory inclusions in carbonaceous chondrites. *Geochim. Cosmochim. Acta* **110**, 190–215 (2013).
26. A. W. Needham, S. Messenger, J. Han, L. P. Keller, Corundum–hibonite inclusions and the environments of high temperature processing in the early Solar System. *Geochim. Cosmochim. Acta* **196**, 18–35 (2017).
27. T. Ushikubo, T. J. Tenner, H. Hiyagon, N. T. Kita, A long duration of the ^{16}O -rich reservoir in the solar nebula, as recorded in fine-grained refractory inclusions from the least metamorphosed carbonaceous chondrites. *Geochim. Cosmochim. Acta* **201**, 103–122 (2017).
28. S. B. Simon, A. N. Krot, K. Nagashima, L. Kööp, A. M. Davis, Condensate refractory inclusions from the CO3.00 chondrite Dominion Range 08006: Petrography, mineral chemistry, and isotopic compositions. *Geochim. Cosmochim. Acta* **246**, 109–122 (2019).
29. T. R. Ireland, Presolar isotopic and chemical signatures in hibonite-bearing refractory inclusions from the Murchison carbonaceous chondrite. *Geochim. Cosmochim. Acta* **54**, 3219–3237 (1990).
30. E. J. Catanzaro, T. J. Murphy, E. L. Gardner, W. R. Shields, Absolute isotopic abundance ratios and atomic weight of magnesium. *J. Res. Natl. Bur. Stand.* **70A**, 453–458 (1966).
31. L. Kööp, A. M. Davis, D. Nakashima, C. Park, A. N. Krot, K. Nagashima, T. J. Tenner, P. R. Heck, N. T. Kita, A link between oxygen, calcium and titanium isotopes in ^{26}Al -poor hibonite-rich CAIs from Murchison and implications for the heterogeneity of dust reservoirs in the solar nebula. *Geochim. Cosmochim. Acta* **189**, 70–95 (2016).
32. J. N. Grossman, A. J. Brearley, The onset of metamorphism in ordinary and carbonaceous chondrites. *Meteorit. Planet. Sci.* **40**, 87–122 (2005).
33. D. York, N. M. Evensen, M. L. Martínez, J. De Basabe Delgado, Unified equations for the slope, intercept, and standard errors of the best straight line. *Am. J. Phys.* **72**, 367–375 (2004).
34. S. S. Russell, G. R. Huss, A. J. Fahey, R. C. Greenwood, R. Hutchison, G. J. Wasserburg, An isotopic and petrologic study of calcium-aluminum-rich inclusions from CO3 Meteorites. *Geochim. Cosmochim. Acta* **62**, 689–714 (1998).
35. F. A. Podosek, E. K. Zinner, G. J. Macpherson, L. L. Lundberg, J. C. Brannon, A. J. Fahey, Correlated study of initial $^{87}\text{Sr}/^{86}\text{Sr}$ and Al-Mg isotopic systematics and petrologic properties in a suite of refractory inclusions from the Allende meteorite. *Geochim. Cosmochim. Acta* **55**, 1083–1110 (1991).
36. N. T. Kita, Q.-Z. Yin, G. J. MacPherson, T. Ushikubo, B. Jacobsen, K. Nagashima, E. Kurahashi, A. N. Krot, S. B. Jacobsen, ^{26}Al - ^{26}Mg isotope systematics of the first solids in the early solar system. *Meteorit. Planet. Sci.* **48**, 1383–1400 (2013).
37. K. Lodders, Solar System abundances and condensation temperatures of the elements. *Astrophys. J.* **591**, 1220–1247 (2003).
38. F. M. Richter, P. E. Janney, R. A. Mendybaev, A. M. Davis, M. Wadhwa, Elemental and isotopic fractionation of Type B CAI-like liquids by evaporation. *Geochim. Cosmochim. Acta* **71**, 5544–5564 (2007).
39. A. P. Boss, Evolution of the solar nebula. IX. Gradients in the spatial heterogeneity of the short-lived radioisotopes ^{60}Fe and ^{26}Al and the stable oxygen isotopes. *Astrophys. J.* **739**, 61 (2011).
40. F. C. Pignatelli, S. Charnoz, M. Chaussidon, E. Jacquet, Making the planetary material diversity during the early assembling of the Solar system. *Astrophys. J. Lett.* **867**, L23 (2018).
41. L. Kööp, A. M. Davis, A. N. Krot, K. Nagashima, S. B. Simon, Calcium and titanium isotopes in refractory inclusions from CM, CO, and CR chondrites. *Earth Planet. Sci. Lett.* **489**, 179–190 (2018).
42. L. Yang, F. J. Ciesla, The effects of disk building on the distributions of refractory materials in the solar nebula. *Meteorit. Planet. Sci.* **47**, 99–119 (2012).
43. L. E. Kristensen, M. M. Dunham, Protostellar half-life: new methodology and estimates. *Astron. Astrophys.* **618**, A158 (2018).
44. M.-C. Liu, K. D. McKeegan, T. M. Harrison, G. Jarzebinski, L. Vltava, The Hyperion-II radio-frequency oxygen ion source on the UCLA *ims*1290 ion microprobe: Beam characterization and applications in geochemistry and cosmochemistry. *Int. J. Mass Spec.* **424**, 1–9 (2018).
45. A. M. Davis, F. M. Richter, R. A. Mendybaev, P. E. Janney, M. Wadhwa, K. D. McKeegan, Isotopic mass fractionation laws for magnesium and their effects on ^{26}Al - ^{26}Mg systematics in solar system materials. *Geochim. Cosmochim. Acta* **158**, 245–261 (2015).

Acknowledgments: Constructive comments from M. Chaussidon, A. Davis, and an anonymous reviewer greatly improved the presentation of this manuscript. We also thank K. McKeegan and E. Young for the inspiring discussions. G. Jarzebinski and L. Vltava are thanked for keeping the *ims*-1290 in top condition. **Funding:** This work is supported by NASA grants 80NSSC18K0602 (to M.-C.L.) and NNX15AD28G (to A.J.B.) and LPI contribution no. 2208. The UCLA ion microprobe facility is partially supported by a grant from the NSF Instrumentation and Facilities program, for which the authors are grateful. **Author contributions:** M.-C.L. designed the research; J.H. and A.J.B. characterized the samples and acquired bulk chemical compositions of certain inclusions; M.-C.L. and A.T.H. performed the research; M.-C.L. interpreted the data; and M.-C.L., J.H., A.J.B., and A.T.H. wrote the paper. **Competing interests:** The authors declare that they have no competing interests. **Data and materials availability:** All data needed to evaluate the conclusions in the paper are present in the paper and/or the Supplementary Materials. Additional data related to this paper may be requested from the authors.

Submitted 10 December 2018
 Accepted 8 August 2019
 Published 11 September 2019
 10.1126/sciadv.aaw3350

Citation: M.-C. Liu, J. Han, A. J. Brearley, A. T. Hertwig, Aluminum-26 chronology of dust coagulation and early solar system evolution. *Sci. Adv.* **5**, eaaw3350 (2019).